Geometry Optimization of Charged Molecules in an External Electric Field Applied to F −,H 2 O and I −,H 2 O

2 **AUTHORS**, INCLUDING:

Visvaldas Kairys
Vilnius University

47 PUBLICATIONS **1,121** CITATIONS

Geometry Optimization of Charged Molecules in an External Electric Field Applied to F⁻·H₂O and I⁻·H₂O

Visvaldas Kairys and John D. Head*

Department of Chemistry, University of Hawaii, 2545 The Mall, Honolulu, Hawaii 96822

Received: July 14, 1997; In Final Form: November 12, 1997

A general constrained geometry optimization procedure for charged molecules in an external electric field is developed. The procedure uses constraints to neutralize the resultant net force between the charged molecule and the external electric field. Three different constraints are explicitly considered: (1) a fixed center of coordinates, (2) a fixed center of mass, and (3) a fixed single atom. Field-dependent optimized geometries and vibrational frequencies for F⁻·H₂O and I⁻·H₂O are obtained and shown to be constraint-dependent. The constrained center of coordinates appears to simulate the charged system at static equilibrium in the electric field. The fixed atom constraint models the situation when an atom becomes attached to a more extended substrate. The center-of-mass constraint gives optimized structures that are mass sensitive and intermediate between those obtained with the other two constraints. The constrained geometry optimization procedure has applications to modeling different environments on electrode surfaces.

1. Introduction

Recently there has been a growing effort to theoretically model the atomic interactions occurring on electrode surfaces. Several investigators used the ab initio cluster model to represent the surface of a metallic electrode.[1−4] Another popular approach is based on the molecular dynamics type calculations.[5−7] Although we do not discuss this second approach in any detail, it is worth noting that the interaction potentials used in molecular dynamics are often derived from the ab initio cluster calculations. Typically in the ab initio cluster calculations the electronic structure of an adsorbate on a cluster of metal atoms is investigated, where the cluster simulates the surface of the metal electrode. In this procedure, it is usually assumed that the varying electrode potential can be modeled by adding or subtracting an electron to the whole system. Unfortunately, the computational demands of the cluster calculations increase rapidly if the adsorbate is a complicated system of atoms. A simpler solution is to replace the effect of the charged cluster by the electric field this cluster creates. Some justification for this approximation has recently been given by Lambert in a review of the vibrational Stark effect.[8]

A recent goal of our work has been to use ab initio cluster calculations to model water[9,10] and solvated halide ions at electrode surfaces.[11] In the course of this work we realized there were not many calculations that reported geometries and vibrational frequencies for charged molecules in external electric fields. Combariza et al. have reported extensive and density functional calculations investigating the halide ions F⁻ and I⁻ interacting with one or several water molecules.[12−15] The geometries of these polyatomic molecules were determined in the usual fashion by evaluating analytic energy derivatives and making use of an efficient geometry optimization algorithm.[16−18] For a molecule in an external homogeneous electric field the appropriate analytical first derivatives can be calculated by adding the electron- and nucleus-field interaction terms to the

one-electron Hamiltonian. Duran et al. have also derived expressions for the analytic second-order derivatives for closed-shell restricted Hartree−Fock functions with an applied uniform electric field for neutral molecular systems.[19] However, a molecule with net charge Q in an external electric field **F** will have a residual force Q**F** preventing the determination of an equilibrium geometry where all of the energy derivatives are zero. Hermansson et al. have investigated the optimum geometry and vibrational frequency for OH⁻ and CN⁻ in a homogeneous external electric field as well as in electric fields generated by point charges placed around the ions.[20−28] The calculations are used to simulate the ionic effects from crystalline environments on the OH bond length and stretching vibration in water and OH⁻. Similar trends in the vibrational frequency changes with varying of electric field strength were found using homogeneous electric fields and the point charges. The OH⁻ and CN⁻ optimum geometries and vibrational frequencies were obtained from the potential energy curve computed from single-point energy calculations rather than using a derivative-based optimization method.[28] Several papers by Bertrán and co-workers have discussed the influence of an electric field on the reactions pathways for charged F⁻ + CH₃F → FCH₃ + F⁻ and [CH₃−H−CH₃]⁺.[29−31] They compute the energies and analytical first derivatives by adding the required interaction terms to the one-electron Hamiltonian, but they do not clearly state how the net force on the system is treated in their geometry optimizations.

In this paper, we investigate the optimal geometries for a charged halide ion hydrated with a single molecule in electric fields with strengths similar to those existing near an electrode surface. The paper is organized as follows. In the Method section we derive the gradient expressions necessary for optimizing the geometry of a charged molecular system in an external electric field. Due to the resultant net force on the charged molecule from its interaction with the electric field, a general constrained optimization procedure is developed and illustrated for three specific types of constraints. The computational details used in the ab initio calculations are also given in the Method section. In the Results and Discussion section

* Tel: (808)-956-5787. Fax: (808)-956-5908. E-mail: johnh@gold.chem.hawaii.edu.

geometries, binding energies, and vibrational frequencies for $F^- \cdot H_2O$ and $I^- \cdot H_2O$ computed for the different optimization constraints and electric field strengths are presented. A summary and concluding remarks are made in the final section of the paper.

2. Method

2.1. Constrained Geometry of a Charged Molecule in an Electric Field. In this section we discuss the conditions necessary to be able to assign equilibrium coordinate positions to a molecular system that has a net charge Q in an external electric field $\mathbf{F}$. Formally, the charged molecule is not strictly at equilibrium since the net charge results in a residual force on the system and the gradient vector will not go to zero. We optimize the geometry of the molecule by applying constraints to the nuclear coordinates that balance against the total force generated from the net charge and the electric field. Even though the total energy $E(\mathbf{F})$ of the system has a linear dependence on translation of the molecule along the electric field $\mathbf{F}$ direction, the energy first and higher derivatives are invariant to these translations, making it possible to define a unique optimized structure for the system. We optimize the geometry of the molecule by minimizing the energy while applying constraints to the nuclear coordinates that balance against the total force generated from the net charge and the external electric field. Suitable constraints take the general form

$$\sum_i q_i c_{i\alpha} = C_\alpha \tag{1}$$

where q_i are the nuclear coordinates, $c_{i\alpha}$ are the constraints, and C_α is the quantity held constant. The subscript α signifies the optimization may involve more than one constraint.

Using Lagrange's method of undetermined multipliers, the optimum energy can be obtained by minimizing

$$G = E(\mathbf{F}) + \lambda(\sum_i q_i c_i - C) \tag{2}$$

A stationary point is obtained when the derivatives

$$\frac{\partial G}{\partial q_i} = \frac{\partial E(\mathbf{F})}{\partial q_i} + \lambda c_i \tag{3}$$

are zero. This produces the interesting result

$$\frac{\partial E(\mathbf{F})}{\partial q_i} = -\lambda c_i \tag{4}$$

where the final E gradient for the optimized structure depends on the constraint being used. In order for the displacements of the molecular coordinates to be in a space orthogonal to the constraints, one can show that

$$\lambda = -\frac{\sum_i c_i \partial E(\mathbf{F})/\partial q_i}{\sum_i c_i^2} \tag{5}$$

should be used in eq 3.[32]

In this paper we consider three different types of constraints.

1. Fixed Center of Coordinates. Here $\sum_i^N q_i$ in the x, y, and z directions are kept constant and all the constraints c_i are unity. The correction λc_i for each gradient is then

$$\lambda c_i = -\frac{1}{N}\sum_i^N \frac{\partial E(\mathbf{F})}{\partial q_i} \tag{6}$$

2. Fixed Center of Mass. The mass-weighted coordinates $\sum_i^N q_i m_i$ are kept constant, with c_i taken to be the mass of the nucleus associated with coordinate q_i. The expression for λc_i is

$$\lambda c_i = -\frac{m_i}{\sum_i^N m_i^2}\sum_i^N m_i \frac{\partial E(\mathbf{F})}{\partial q_i} \tag{7}$$

3. Fixed Single Atom in Space. This constraint corresponds to zeroing out the analytical energy gradient on the fixed atom i so that

$$\frac{\partial G}{\partial q_i} = \frac{\partial E(\mathbf{F})}{\partial q_i} + \lambda c_i = 0 \tag{8}$$

while for the unconstrained atoms $\partial G/\partial q_j = \partial E(\mathbf{F})/\partial q_j$. In the present work we only consider constraining the halide ion.

These three optimization constraints simulate different physical situations. Equations 4 and 6 indicate that the optimized structure obtained with the center of coordinates constraint appears to produce a static equilibrium structure, with the net force on the charged molecular system being evenly distributed as equal magnitude energy gradients on each of the atoms. On the basis of the fact that the usual approach to treat the dynamics of a system is to separate the center-of-mass motion from the relative motion, we expected the center-of-mass, type 2, constraint to most closely resemble the actual geometry the charged molecule adopts in free space while undergoing translational motion from the external force due to the electric field. However, at the stationary point eq 4 requires the energy gradients on the ith atom to be proportional to its mass. Eventually, if the dynamical system is able to relax to a static situation, it is not clear why a heavier atom should have a greater gradient. At present we are uncertain of the physical situation the type 2 constraint models, apart from maintaining the center-of-mass at one location. Constraint 3, where a single atom is constrained, approximates the situation where the constrained atom somehow becomes attached to a more extended substrate. We have already been extensively using this type of constraint in the partial geometry optimization of adsorbates on surfaces using cluster calculations.[9,10,33,34] In the Results and Discussion section we demonstrate that constraints 1 and 3 correspond to different limiting conditions for the center-of-mass constraint and discuss further the merits of each constraint type.

All of the present calculations have been performed using Cartesian coordinates. However, the same geometry constraints on a charged molecule can be defined for an optimization in the more chemically intuitive internal coordinates, where the geometry is expressed in terms of bond lengths and angles.[35,36] In the geometry optimization of a neutral molecule the same final geometry is produced regardless of whether internal or Cartesian coordinates are used, although the rate of convergence of the optimization may be coordinate-dependent.[37-39] Internal coordinates automatically factor out the translational and rotational degrees of freedom for the molecule, and these would

Geometry Optimization of Charged Molecules

J. Phys. Chem. A, Vol. 102, No. 8, 1998 **1367**

include the net force on the charged molecule in an electric field. Nonetheless, the above three Cartesian constraints can still be active. In a typical geometry optimization using internal coordinates, the energy derivatives are first evaluated with respect to the Cartesian coordinates of the molecule; the derivatives are then transformed to the internal coordinates and used to generate a new set of internal coordinates closer to the optimized geometry. These new internal coordinates are then back transformed to the Cartesian coordinates. It is this back transformation step that determines the type of constraint being applied in the optimization. A type 1 constraint will be invoked if the molecules center of coordinates is preserved, a type 2 constraint when the center-of-mass is kept at the same position, and the type 3 constraint if the molecule is rebuilt with one of the atoms kept at the origin. Thus, although the above constraints introduced corrections to the Cartesian gradients, it is how the coordinates of the molecule are organized that determines the optimization type. Hermansson et al. in their fitting procedure to obtain the optimum OH^- bond length in the external electric field keep the center-of-mass position constant and are effectively performing a type 2 optimization.[28] Whereas the calculations by Bertrán and co-workers on $CH_3F_2^-$ and $C_2H_7^+$ were probably performed using internal coordinates, the authors do not specify how the coordinates were organized, and as a consequence it is not clear which optimization constraint is being used in their calculations.[29-31]

2.2. Computational Details. All calculations were performed using the GAMESS ab initio program package.[40] The energy gradient routines in the GAMESS program were modified slightly to produce the correct gradient for a charged molecule in an electric field and to incorporate the appropriate optimization constraints using eqs 3−8. Rather extensive basis sets are needed to compute reliable properties of negatively charged molecules. For the F, O, and H atoms Pople's 6-31++G** basis sets were used.[41-44] The averaged relativistic effective potential (AREP) of Christiansen et al.[45] was used for the I atom, with the outermost core 4d electrons as well as the valence subshells 5s and 5p included into the valence space. In addition, we included a diffuse d function with an exponent 0.266[46] and a diffuse sp function (exponent 0.0368[46]) to produce a $(4s4p5d)/[3s3p2d]$ basis for I. The present energy and gradient calculations were performed at the RHF SCF level.

The frequencies corresponding to the normal vibrational modes were calculated in the usual way, by diagonalization of the mass-weighted Hessian matrix, which was computed numerically using the GAMESS program. Notably, for the constraints 1 and 2 the calculated frequencies depend only on the atomic coordinates input into the program, since the fixed center-of-coordinates and fixed center-of-mass constraints generate constant corrections to the gradient. The fixed atom constraint was treated differently, and we assume the fixed atom does not participate in the collective vibrations of the molecule. In this case, the mass-weighted Hessian matrix was formed using only the free atoms. The Hessian matrix diagonalization produces $3N-3$ vibrations, with two of the lowest frequencies corresponding to frustrated translations of the unconstrained part of the molecule in directions perpendicular to the electric field vector **F**. For an unconstrained nonlinear fragment, there is a third low-frequency mode corresponding to a frustrated rotation around an axis parallel to **F**.

3. Results and Discussion

The $F^-\cdot H_2O$ and $I^-\cdot H_2O$ equilibrium geometries obtained for different electric field strengths using the three constraint types

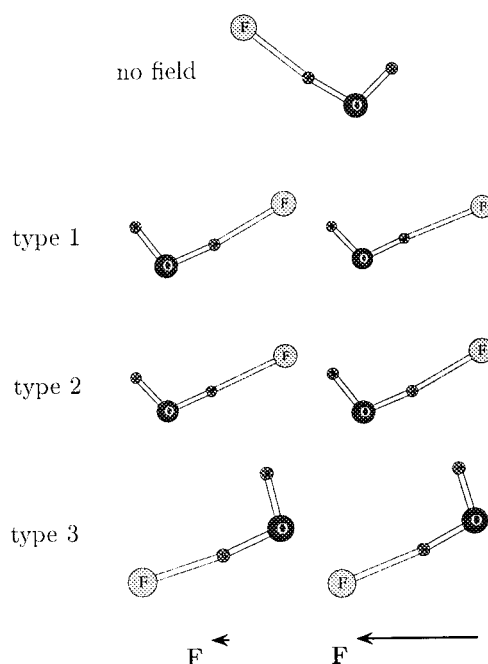**Figure 1.** Optimized $F^-\cdot H_2O$ geometries obtained for the 0.001 and 0.01 au electric field strengths with different constraint types.

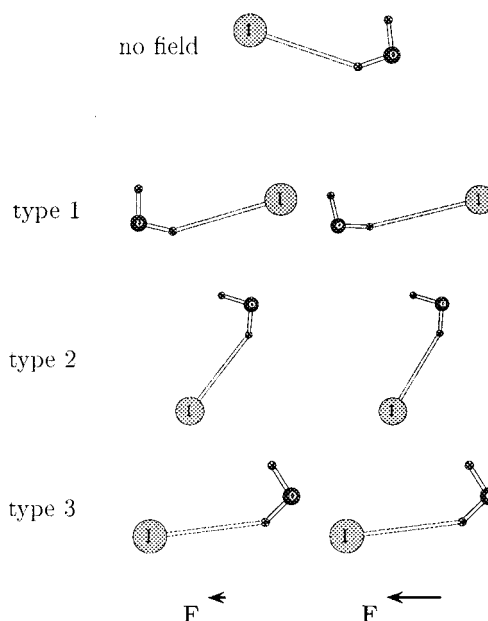**Figure 2.** Optimized $I^-\cdot H_2O$ geometries obtained for the 0.001 and 0.003 au electric field strengths with different constraint types.

are shown in Figures 1 and 2. Due to the absence of a net force, the three constraint types produce identical optimized $F^-\cdot H_2O$ and $I^-\cdot H_2O$ geometries when there is a zero external electric field. The zero-field $F^-\cdot H_2O$ optimized geometry reflects the expected strong H bonding between the water and F, causing the F−H−O angle to be almost linear. In $I^-\cdot H_2O$ the H bonding is much weaker and the I−H−O angle is bent. The I−H−O bending has a simple electrostatic origin due to the dipole moment of the water trying to line up with the electric field lines from the I^- point charge. Our zero-field calculations reproduce the SCF geometries obtained previously by Combariza et al.[12-15] Combariza et al. also report structures that include some electron correlation by using density functional theory and second-order Møller−Plesset perturbation (MP2) theory but find only slightly stronger halide−water interactions and the F-to-H distance shortened by about 0.1 Å. Zhan and

TABLE 1: Geometries for Isolated Water, $F^-\cdot H_2O$, and $I^-\cdot H_2O$ (in Å and deg) and X^--to-H_2O Binding Energies (kcal/mol) Obtained with Different Electric Field Strengths F (au) Using the Three Different Optimization Constraints

constraint	$|\mathbf{F}|$	$d(X-H_\alpha)$	$d(O-H_\alpha)$	$d(O-H_\beta)$	$XH_\alpha O$	$H_\alpha OH_\beta$	BE
			H_2O				
	0.000		0.943	0.943		107.1	
	0.001		0.943	0.943		106.9	
	0.003		0.944	0.944		106.7	
	0.01		0.945	0.945		105.7	
			$F^-\cdot H_2O$				
	0.000	1.503	1.000	0.942	172.5	103.5	24.7
type 1	0.001	1.520	0.997	0.942	173.4	104.0	23.6
	0.003	1.558	0.991	0.942	175.3	105.0	21.4
	0.01	1.773	0.970	0.943	176.3	108.0	12.9
type 2	0.001	1.517	0.997	0.942	173.0	103.8	23.7
	0.003	1.546	0.992	0.942	174.1	104.4	21.5
	0.01	1.666	0.977	0.942	179.1	106.5	13.9
type 3	0.001	1.495	1.003	0.942	172.4	103.3	25.1
	0.003	1.476	1.009	0.942	172.3	102.9	25.8
	0.01	1.385	1.043	0.942	172.7	101.4	28.6
			$I^-\cdot H_2O$				
	0.000	3.013	0.950	0.944	142.0	102.9	9.1
type 1	0.001	3.044	0.950	0.943	150.0	103.8	7.9
	0.003	3.380	0.948	0.943	164.1	105.7	4.8
type 2	0.001	2.966	0.951	0.944	147.3	103.1	9.1
	0.003	2.914	0.951	0.944	154.0	103.4	9.0
	0.01	2.849	0.954	0.944	166.1	103.9	8.3
type 3	0.001	3.008	0.950	0.944	141.9	102.7	9.3
	0.003	2.993	0.951	0.944	142.3	102.3	9.7
	0.01	2.963	0.955	0.946	141.8	100.7	11.4

Iwata in MP2 calculations obtained essentially the same $X^-\cdot H_2O$ results as Combariza et al. using a slightly inferior quality basis set.[47] We have also obtained $X^-\cdot H_2O$ results similar to Combariza's in preliminary MP2 calculations, but since we are more interested in the results from the application of the different optimization constraints, we only present results of the Hartree—Fock calculations in this paper.

For the nonzero electric field the $X^-\cdot H_2O$ geometry appears to be determined by a competition between H_2O dipole alignment with the external field $\mathbf{F}$ and either the halide H-bond strength or the electric field generated by X^-. For the water—fluoride complex in the electric field, there are two distinct geometry types produced by using the three different optimization constraints. For constraints 1 and 2, F^- as the most negatively charged species in the system is attracted to the positive source of the electric field and the water dipole is almost perpendicular to the electric field. For the type 3 constraint, where the F^- is fixed in space, the F^--water direction is reversed relative to the type 1 and 2 geometries. The water dipole moment is now more closely aligned with the electric field direction, but this resulting structure may be coupled with the approximately $0.1e$ charge lost from F^-, causing the H_2O molecule to be attracted to the positive source of the electric field. Table 1 shows the F—H bond length to be the geometrical parameter most sensitive to the electric field, increasing (decreasing) with the type 1 and 2 (type 3) constraints. The length of the OH bond neighboring F^- is also fairly sensitive to the electric field and is appreciably longer than the 0.943-Å OH bond length computed for the isolated water molecule. In contrast, the isolated water OH distance increases only to 0.945 Å in an electric field of 0.010 au.

Two geometry types are also found for $I^-\cdot H_2O$ in the electric field. However, because of the much higher I atomic mass relative to F, the optimized geometries obtained with the center-of-mass and the fixed I^- constraints now resemble each other for low electric fields. The much smaller differences in the F, O, and H masses produce closer similarities between the type

1 and 2 optimized geometries for $F^-\cdot H_2O$. Somewhat surprisingly, the center-of-mass constraint results in the I^- being on the negative side of the electric field. In stronger electric fields, with the I^- held fixed the water dipole becomes almost parallel with the electric field, while the center-of-mass constraint produces an optimized geometry which still resembles its low electric field geometry. The center-of-coordinates constraints produce $I^-\cdot H_2O$ geometries similar to the type 1 and type 2 geometries obtained for $F^-\cdot H_2O$. The I^--to-H distance is also the geometrical parameter most sensitive to the electric field, increasing (decreasing) with the type 1 (type 2 and 3) constraints. These results serve as a warning that when performing a geometry optimization on a charged molecule in an electric field that although a unique final structure will be computed, the structure obtained will be dependent on the optimization constraint used to balance the net force on the molecule.

In Table 1 we also list X^--to-H_2O binding energies for the optimized geometries obtained using the different constraints and different external electric fields. Since the energy of the charged system in an electric field is coordinate-dependent, we have computed a coordinate-independent binding energy by using

$$BE(X^- + H_2O, \mathbf{F}) = -E(X^-\cdot H_2O, \mathbf{F}) + E(X^-, \mathbf{F}) + E(H_2O, \mathbf{F}) \quad (9)$$

where the energies $E(X^-\cdot H_2O, \mathbf{F})$ for the halide—water system, $E(X^-, \mathbf{F})$ for the halide ion taken to have the same coordinates as the X^- in the $X^-\cdot H_2O$ geometry optimization calculation, and $E(H_2O, \mathbf{F})$ for the optimized water geometry are all computed for the electric field $\mathbf{F}$. Consistent with the strong H bond between water and F^-, Table 1 shows $F^-\cdot H_2O$ to be much more strongly bound than $I^-\cdot H_2O$. Our calculated binding energies are in good agreement with the 23 and 10 kcal/mol enthalpy changes determined experimentally in the solvation of F^- and I^- by a single water molecule.[48] Table 1 also shows that the X^--to-water binding energy for the type 1 optimized geometry decreases in stronger electric fields. Eq 4 requires the net force on the type 1 structure to be evenly spread over all the atoms, causing a lengthening of the X^--to-H bond with increasing electric field. In contrast, the type 3 optimized structure, with X^- held fixed, has zero energy gradients on the water atoms, resulting in a slight shortening of the X^--to-H distance and relatively small binding energy changes. Increasing the electric field strength for the center-of-coordinates, type 1, constraint eventually causes the bond between the halide and water to break. The critical electric field strength turned out to be 0.013 au for $F^-\cdot H_2O$ and 0.004 au for $I^-\cdot H_2O$ (1 au = 5.14 $\times 10^{11}$ V/m) and is consistent with the greater solvation energy for F^-. It is interesting to see the X^--to-H distance is stretched by over 0.25 Å before breaking.

The vibrational frequencies calculated at the optimized $F^-\cdot H_2O$ and $I^-\cdot H_2O$ geometries for the different constraints and electric field strengths are given in Table 2. Generally, the forms of each of the vibrational modes obtained with the three different optimization constraints are identical to each other, although, as we point out below, the frequency values do change with the external electric field strength and these changes are dependent on the geometry constraint type. The two modes having the highest frequencies, ν_1 and ν_2, correspond to the water OH stretches. In all calculations, the ν_1 mode, which corresponds to the nonbonded OH stretch, is only slightly shifted from antisymmetric and symmetric stretching frequencies computed at 4269 and 4147 cm^{-1} for isolated water using the

Geometry Optimization of Charged Molecules

J. Phys. Chem. A, Vol. 102, No. 8, 1998 **1369**

TABLE 2: Vibrational Frequencies Obtained for Isolated Water, F⁻·H₂O, and I⁻·H₂O at Different External Electric Field Strengths F (au) Using the Three Different Optimization Constraints. The Frequencies Are in cm⁻¹

system	constraint	$|\mathbf{F}|$	ν_1	ν_2	ν_3	ν_4	ν_5	ν_6
					normal modes			
H₂O		0.000	4269	4147	1728			
		0.003	4266	4146	1732			
		0.001	4261	4144	1739			
		0.01	4241	4135	1760			
F⁻·H₂O		0.000	4211	3040	1862	1164	555	321
	type 1	0.001	4212	3105	1860	1146	555	311
		0.003	4214	3232	1853	1110	556	289
		0.01	4214	3659	1802	939	540	201
	type 2	0.001	4214	3098	1860	1149	553	314
		0.003	4217	3206	1857	1119	550	298
		0.01	4225	3528	1830	1007	539	237
	type 3	0.0	4211	3039	1861	1159	550	231
		0.001	4210	2990	1862	1172	557	232
		0.003	4206	2879	1864	1197	570	236
		0.01	4192	2267	1835	1308	614	248
I⁻·H₂O		0.000	4215	4087	1782	565	148	96
	type 1	0.001	4223	4081	1778	544	184	84
		0.003	4237	4097	1761	464	210	55
	type 2	0.001	4215	4069	1784	576	194	99
		0.003	4213	4045	1787	591	246	103
		0.01	4201	4004	1798	620	337	194
	type 3	0.0	4215	4087	1782	565	148	90
		0.001	4211	4080	1785	579	158	91
		0.003	4205	4064	1789	606	182	93
		0.01	4181	4002	1802	687	236	100

same basis set. In contrast ν_2, involving the vibration of the H atom between O and X⁻, shows much larger shifts from the isolated water OH stretching frequencies. Even in the absence of an external electric field, the F⁻·H₂O ν_2 frequency is dramatically shifted from the isolated water stretching frequency presumably because of large H-bonding effects. The water bending mode is responsible for the ν_3 frequency, and again the F⁻·H₂O frequency shows the largest shift from the isolated water bending frequency computed at 1728 cm⁻¹. Modes ν_4 and ν_5 are due to bending vibrations of O–H–X perpendicular and coplanar, respectively, to the plane of the X⁻·H₂O ion. The higher ν_4 and ν_5 frequencies for F⁻·H₂O relative to I⁻·H₂O correlate with the stronger H-to-X⁻ interaction. The X⁻-to-H stretch is given by ν_6.

Not included in Table 2 are the three additional vibrational frequencies corresponding to the frustrated translations and rotation for the water molecule while constraining the halide atom. For a 0.01-au electric field strength we compute frequencies at 10, 33, and 141 cm⁻¹ for F⁻·H₂O and 5, 15, and 72 cm⁻¹ for I⁻·H₂O with the frustrated rotation having the highest frequency.

In the presence of an external electric field the F⁻·H₂O ν_2 mode is the mode that exhibits the largest and essentially linear Stark effect. However this ν_2 mode is blue-shifted for geometries computed using the center-of-coordinates and center-of-mass constraints where the F–H distance increases with electric field and red-shifted for the geometries computed with F⁻ held fixed with the F–H distance decreasing with electric field. Much weaker Stark shifts occur for F⁻·H₂O modes ν_3–ν_6, but the frequency changes are in the direction opposite those for the ν_2 mode. The ν_2 mode for I⁻·H₂O is only slightly shifted from its isolated water value, and the largest I⁻·H₂O Stark effect occurs for the low-frequency modes ν_4 and ν_5. Similar to what we found in the geometry optimizations, the frequency shifts for constraints 2 and 3 resemble each other, while the center-of-coordinates constraint produces frequency shifts in the opposite direction. At present we do not have a physical

explanation for the origin of the frequency shifts with external electric field or why the different optimization constraints produce different trends in vibrational shifts. Hermansson has correlated the electric field induced frequency shifts to derivatives of the free-molecule and field-induced dipole moment along the vibrating bond direction.[25] If instead one considers the geometry changes with electric field strength and one assumes the vibrational frequency is proportional to bond strength, then the F⁻·H₂O ν_2 mode frequency values are consistent with a strengthening of the O–H bond as the F–H bond length gets longer, thereby reducing the H-bonding between the F⁻ and H. Interestingly this large Stark effect computed for the F⁻·H₂O ν_2 mode should be big enough to be experimentally observed.

4. Summary and Conclusions

A procedure for geometry optimizing charged molecules in an external electric field is presented. The optimization procedure requires the introduction of constraints to counteract the resultant net force due to the interaction between the electric field and the charged molecule. The general forms of the constraints are given by eq 1, and we have presented three specific constraint types: (1) fixed center of coordinates, (2) fixed center of mass, and (3) fixed single atom. All of the different constraint types produce identical optimized geometries for either neutral molecules in an electric field or charged molecules in the absence of an electric field. However, the optimized structures of charged molecules in an electric field are dependent on the type of constraint used. The appropriate constraint to use depends on the physical situation being modeled. The center-of-coordinates, type 1, constraint appears best suited to describe a charged molecule in free space. The single fixed atom constraint should be useful for modeling the situation where one of the atoms in the charged molecule starts to adsorb on a surface or electrode. The center-of-mass constraint does not appear to be physically useful. The same type of constraints can also be defined for internal coordinates.

The geometry optimization procedure was applied to F⁻·H₂O and I⁻·H₂O. For a particular electric field strength, the different constraints produced different optimized geometries. Generally, the resulting structures and binding energies are consistent with F⁻ forming a much stronger H-bond than I⁻ with water. Significant structural changes occur with an applied external electric field. The type 1 constraint produces optimized structures with weaker halide ion to water bonding as the electric field strength is increased. This can be attributed to the type 1 constraint causing the net force to be evenly distributed over all the atoms. At high enough electric fields the halide ion and water break apart. The much higher field strength needed to break apart F⁻·H₂O versus I⁻·H₂O correlates with the greater F⁻ solvation energy. The type 3 constraint causes the net force to be centered at the halide ion, thereby affecting less the halide ion to water bonding. The center-of-mass, type 2, constraint produces optimized structures intermediate between those from the type 1 and 3 constraints with the actual structural details being dependent on the relative masses of the atoms composing the system.

The vibrational frequencies for F⁻·H₂O and I⁻·H₂O with different external electric field strengths were also calculated. The large F⁻-to-water H-bonding is again the probable cause for the large OH frequency shift from the isolated water value. The vibrational frequencies vary with the external electric field strength to give rise to linear Stark effects. The largest frequency shifts are found for the ν_2 mode involving the

1370 *J. Phys. Chem. A, Vol. 102, No. 8, 1998*

Kairys and Head

vibration of H between O and X$^-$. The ν_2 frequency increases as the optimized H-to-X$^-$ distance becomes longer. The calculated F$^-\cdot$H$_2$O Stark effect for the ν_2 mode is large enough to suggest it could be experimentally observed.

References and Notes

(1) Seitz-Beywl, J.; Poxleitner, M.; Probst, M. M.; Heinzinger, K. *Int. J. Quantum. Chem.* **1992**, *42*, 1141.

(2) Kuznetsov, An. M. *Electrochim. Acta* **1995**, *40*, 2485.

(3) Tóth, G.; Spohr, E.; Heinzinger, K. *Chem. Phys.* **1995**, *200*, 347.

(4) Pacchioni, G. *Electrochim. Acta* **1996**, *41*, 2285.

(5) Tóth, G.; Heinzinger, K. *Chem. Phys. Lett.* **1995**, *245*, 48.

(6) Philpott, M. R.; Glosli, J. N.; Zhu, S.-B. *Surf. Sci.* **1995**, *335*, 442.

(7) Böcker, J.; Nazmutdinov, R. R.; Spohr, E.; Heinzinger, K. *Surf. Sci.* **1995**, *335*, 372.

(8) Lambert, D. K. *Electrochim. Acta* **1996**, *41*, 623 and references therein.

(9) Jin, S.; Head, J. D. *Surf. Sci.* **1994**, *318*, 204.

(10) Calvin, M. D.; Head, J. D.; Jin, S. *Surf. Sci.* **1996**, *345*, 161.

(11) Kairys, V. Ph.D. Thesis, University of Hawaii, 1997.

(12) Combariza, J. E.; Kestner, N. R.; Jortner, J. *Chem. Phys. Lett.* **1994**, *221*, 158.

(13) Combariza, J. E.; Kestner, N. R. *J. Phys. Chem.* **1994**, *98*, 3513.

(14) Combariza, J. E.; Kestner, N. R.; Jortner, J. *J. Chem. Phys.* **1994**, *100*, 2851.

(15) Combariza, J. E.; Kestner, N. R. *J. Phys. Chem.* **1995**, *99*, 2717.

(16) Schlegel, H. B. *Adv. Chem. Phys.* **1987**, *67*, 249.

(17) Head, J. D.; Weiner, B.; Zerner, M. C. *Int. J. Quantum Chem.* **1988**, *33*, 177.

(18) Head, J. D.; Zerner, M. C. *Adv. Quantum Chem.* **1989**, *20*, 239.

(19) Duran, M.; Andrés, J. L.; Lledós, A.; Bertrán, J. *J. Chem. Phys.* **1989**, *90*, 328.

(20) Hermansson, K. *J. Chem. Phys.* **1991**, *95*, 3578.

(21) Hermansson, K. *Chem. Phys.* **1992**, *159*, 67.

(22) Ojamäe, L.; Hermansson, K. *J. Chem. Phys.* **1992**, *96*, 9035.

(23) Hermansson, K. *J. Chem. Phys.* **1993**, *99*, 861.

(24) Hermansson, K. *Chem. Phys.* **1993**, *170*, 177.

(25) Hermansson, K. *Int. J. Quantum Chem.* **1993**, *45*, 747.

(26) Hermansson, K. *Chem. Phys. Lett.* **1995**, *233*, 376.

(27) Hermansson, K.; Lindgren, J.; Probst, M. *Chem. Phys. Lett.* **1995**, *233*, 371.

(28) Hermansson, K.; Tepper, H. *Mol. Phys.* **1996**, *89*, 1291.

(29) Andrés, J. L.; Lledós, A.; Duran, M.; Bertrán, J. *Chem. Phys. Lett.* **1988**, *153*, 82.

(30) Mestres, J.; Lledós, A.; Duran, M.; Bertrán, J. *J. Mol. Struct.* (THEOCHEM) **1992**, *260*, 259.

(31) Mestres, J.; Duran, M.; Bertrán, J. *Theor. Chim. Acta* **1994**, *88*, 325.

(32) Gill, P. E.; Murray, W.; Wright, M. H. *Practical Optimization*; Academic Press: New York, 1984.

(33) Head, J. D. *J. Comput. Chem.* **1990**, *11*, 67.

(34) Kairys, V.; Head, J. D. *Surf. Sci.* **1997**, *380*, 283.

(35) Wilson, Jr., E. B.; Decius, J. C.; Cross, P. C. *Molecular Vibrations*; McGraw-Hill: New York, 1955.

(36) Pulay, P.; Fogarasi, G.; Pang, F.; Boggs, J. E. *J. Am. Chem. Soc.* **1979**, *101*, 2550.

(37) Schlegel, H. B. *Int. J. Quantum Chem. Symp.* **1992**, *26*, 243.

(38) Baker, J. *J. Comput. Chem.* **1993**, *14*, 1085.

(39) Eckert, F.; Pulay, P.; Werner, H.-J. *J. Comput. Chem.* **1997**, *18*, 1473.

(40) Schmidt, M. W.; Baldridge, K. K.; Boatz, J. A.; Elbert, S. T.; Gordon, M. S.; Jensen, J. H.; Koseki, S.; Matsunaga, N.; Nguyen, K. A.; Su, S.; Windus, T. L.; Dupuis, M.; Montgomery, J. A., Jr. *J. Comput. Chem.* **1993**, *14*, 1347.

(41) Ditchfield, R.; Hehre, W. J.; Pople, J. A. *J. Chem. Phys.* **1971**, *54*, 54.

(42) Hehre, W. J.; Ditchfield, R.; Pople, J. A. *J. Chem. Phys.* **1972**, *56*, 2257.

(43) Hariharan, P. C.; Pople, J. A. *Theor. Chim. Acta* **1973**, *28*, 213.

(44) Clark, T.; Chandrasekhar, J.; Spitznagel, G. W.; Schleyer, P. v. R. *J. Comput. Chem.* **1983**, *4*, 294.

(45) LaJohn, L. A.; Christiansen, P. A.; Ross, R. B.; Atashroo, T.; Ermler, W. C. *J. Chem. Phys.* **1987**, *87*, 2812.

(46) GAMESS User's Guide; Oct. 30, 1996.

(47) Zhan, C. G.; Iwata, S. *Chem. Phys. Lett.* **1995**, *232*, 72.

(48) Hiraoka, C.; Mizuse, S.; Yamabe, S. *J. Phys. Chem.* **1988**, *232*, 3943.